Determination of the Oligomeric States of Human and Rat Monoamine Oxidases in the Outer Mitochondrial Membrane and Octyl β-D-Glucopyranoside Micelles Using Pulsed Dipolar Electron Spin Resonance Spectroscopy†

Anup K. Upadhyay,‡ Peter P. Borbat,§ Jin Wang,‡ Jack H. Freed,*,§ and Dale E. Edmondson*,‡

Departments of Biochemistry and Chemistry, Emory University, 1510 Clifton Road, Atlanta, Georgia 30322, and Department of Chemistry and Chemical Biology and the Advanced ESR Technology Center, B52 Baker Laboratory, Cornell University, Ithaca, New York 14853

Received October 23, 2007; Revised Manuscript Received December 4, 2007

ABSTRACT: Human monoamine oxidase A (hMAOA) is considered to be unique among mammalian MAOs in having a non-conservative Glu-X-Lys mutation (X being 151 in MAOAs and 142 in MAOB's), which is suggested to be the reason for its monomeric structure. This hypothesis has been tested in this work. A pargyline based nitroxide spin labeled irreversible inhibitor (ParSL) was used as a MAO active site specific spin probe to measure intersubunit distances in detergent (octyl β-D-glucopyranoside, OGP) purified and OMM bound forms by a pulsed dipolar ESR spectroscopic (PDS) technique. In a parallel approach, the covalent flavin cofactor present in the MAO active sites was reduced to its respective anionic flavin semiquinone and used for measuring inter-flavin distances in detergent purified samples. The measured interspin distances are within 0.1−0.3 nm of those estimated from the available dimeric crystal structures of human MAOB and rat MAOA and show that all human and rat MAOs exist as dimers in the OMM. In the OGP micelle, however, human and rat MAOAs exist only partially (≤50%) as dimers, whereas human and rat MAOBs exist entirely as dimers. The Lys-151-Glu mutant of human MAOA and the Glu-142-Lys mutant of human MAOB exhibit similar spectral properties as the corresponding wild-type enzymes. Therefore, no role of the Glu-X residue in stabilizing dimeric structures of MAOs was found. The monomeric crystal structure reported for human MAOA is thus a result of its instability in the OGP micelles. The general applicability of the PDS technique to structural studies of membrane proteins in their native membrane environments and detergent purified forms is discussed.

Monoamine oxidases (MAOs)[1] are outer mitochondrial membrane (OMM) bound flavoenzymes involved in catalyzing the oxidative deamination and subsequent degradation of amine neurotransmitters and dietary amines (*1*). These enzymes thus play important roles in proper functioning of the central nervous system by maintaining the homeostasis of neurotransmitters such as dopamine and serotonin, as well as in metabolizing dietary amines and pharmaceuticals to prevent them from functioning as false neurotransmitters. Non-physiological levels of MAOA and MAOB activities have been implicated in several neurological disorders including Parkinson's disease and Alzheimer's disease (MAOB) and chronic depression (MAOA). MAOs are therefore clinically proven drug targets for the treatment of these disorders (*2*). MAOA has been of particular interest in recent studies because of its involvement in cognitive development in humans. Deletion of the MAOA gene results in phenotypes of mental retardation and aggressive behavior in humans and in mice (*3*−*7*).

The three-dimensional structures of human and rat MAOA (hMAOA and rMAOA, respectively) and human MAOB (hMAOB) have been determined by X-ray crystallography (*8*−*11*). The three enzymes show similarities in overall protein folds but differ in oligomeric states in their crystalline forms. While hMAOA crystallizes as a monomer, both hMAOB and rMAOA are dimeric in their crystalline forms. On the basis of the sequence analyses of human and other mammalian MAOAs and MAOBs (including non-human primates) and structural modeling studies, Andrés et al. (*12*) have proposed that a conserved Glu-X residue (with X being residue 142 in MAOBs and residue 151 in MAOAs) plays a key role in stabilizing the dimeric structures of human and rat MAOs by facilitating the formation of two salt bridges at the subunit interface. On the basis of this hypothesis, they predicted a monomeric structure for hMAOA since it contains a human exclusive non-conservative Lys mutation at this position (Glu-151-Lys). It has been suggested that this human exclusive mutation in hMAOA may be a result of evolutionary pressure with possible unknown functional relevance in the human lineage (*12*). Given the importance

† This work was supported by NIH Grants GM29433 to D.E.E. and P41-RR016292 and R01-EB03150 to J.H.F.

* Corresponding authors. (J.H.F.) Tel.: (607) 255-3647; e-mail: jhf3@cornell.edu. (D.E.E.) Tel.: (404) 727-5972; fax: (404) 727-2738; e-mail: deedmon@emory.edu.

‡ Emory University.

§ Cornell University.

[1] Abbreviations: MAO, monoamine oxidase; OMM, outer mitochondrial membrane; ESR, electron spin resonance; PDS, pulsed dipolar ESR spectroscopy; DEER, double electron−electron resonance; ParSL, pargyline based spin labeled MAO inhibitor; OGP, *n*-octyl β-D-glucopyranoside; PELDOR, pulsed electron−electron double resonance; SNR, signal-to-noise ratio; MEM, maximum entropy method; fwhm, full width at half maximum.

10.1021/bi7021377 CCC: $40.75
Published on Web 01/17/2008

of MAOA in cognitive development (*3*−*6*), this hypothesis indicates some greater implications toward evolutionarily different structural and functional properties of hMAOA as compared to other mammalian MAOAs. Such a suggestion raises questions as to the suitability of using a rat model for the development and testing of MAOA specific inhibitors of clinical importance to human diseases. To date, no experimental data to validate the proposed role of the Glu-X residue in regulating MAO quaternary structures have been reported.

One major factor in structural studies on membrane proteins is the choice of detergent micelles. It is known that the structural and functional properties of membrane proteins vary in different detergent micelles, and therefore, the choice of detergent plays an important role in proper reconstitution of different membrane proteins maintaining their native quaternary structures (*13*, *14*). Discrepancies between the monomeric state observed in the X-ray structure in detergent micelles to the consensus dimeric forms obtained from 2-D crystallization in lipid bilayers and other biochemical methods have been reported for bovine mitochondrial ADP/ATP carriers (*14*−*16*). Such observations raise questions as to whether observed differences in the oligomeric forms between hMAOA (monomer) and rMAOA (dimer) can potentially be due to their differential stabilities in different detergent micelles used for purifications and crystallizations. A comparative analysis of human and rat MAOs thus requires understanding their structural properties in solubilized forms using the same detergent micelles as well as in their OMM bound forms, which will benefit from ongoing efforts of designing hMAOA specific inhibitors with clinical importance and is of intrinsic interest in furthering our knowledge of the solution and membrane structures of membrane associated proteins. Furthermore, this approach will also allow us to investigate the proposed role of the conserved Glu-X residue in regulating the oligomeric states of human and rat MAOs (*12*).

Various biophysical techniques based on fluorescence spectroscopy (*17*, *18*), mass spectrometry (*19*, *20*), dynamic light scattering and hydrodynamic studies (*21*, *22*), and electron microscopy (*14*, *16*) have been successfully applied for structural studies on different oligomeric complexes of soluble and membrane proteins. However, none of these techniques is readily applicable to study structural properties of membrane proteins in their natural membrane bound forms. To the best of our knowledge, only atomic force microscopy (AFM) has been used to determine the dimeric state of rhodopsin in its natural membrane bound form (*23*). However, this study was only possible due to the high abundance of rhodopsin in the disk membranes of the rod cells (>90% of the total disk proteins) (*24*). Therefore, purification and reconstitution in either detergent micelles or artificial lipid bilayers are the primary available methods for structural studies on membrane proteins (*25*). Since the structural properties of membrane proteins are sensitive to their surrounding lipid environments in the membrane (*25*, *26*), the observed results using these current methodologies are dependent on the properties of the detergent micelles or lipid bilayers used in the reconstitution process. Furthermore, fluorescence based techniques such as fluorescence correlation spectroscopy or fluorescence resonance energy transfer (FRET) require labeling the two interacting subunits with two different fluorescence probes to form the donor−acceptor pairs, which is difficult for a homo-oligomeric protein. Standard biochemical techniques involving chemical cross-linking, native gel electrophoresis (BN-PAGE), and size exclusion chromatography have also been reported for determining oligomeric states of different membrane bound proteins (*27*, *28*). However, these biochemical techniques also require extraction of the proteins in detergent buffers prior to analyses. Therefore, understanding the oligomeric forms of membrane proteins, without disrupting their natural membrane environment, is of overall importance in the realm of structural and functional studies on membrane proteins, which so far has not been addressed in adequate detail.

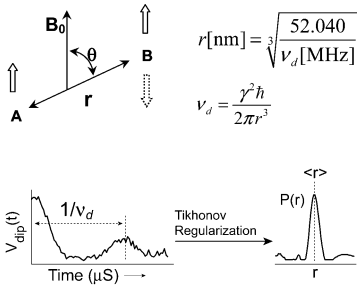

FIGURE 1: Distance measurement by PDS is based on determining the dipolar coupling, $\omega(\mathbf{r}) = 2\pi\nu_d(1 - 3\cos^2\theta)$ between the electron spins A and B of two spin labels. Here, **r** is the vector connecting the spins, and θ is the angle between this vector and the static polarizing magnetic field, $\mathbf{B}_0$. The observer spin A is used to produce an electron spin echo, whose amplitude is modified by selectively flipping spin B, coupled to spin A via electron spin dipole−dipole coupling. The echo amplitude, recorded as a function of time position of the pump pulse, is modulated by electron dipolar coupling between A and B spins. It is then used to reconstruct distances with a suitable method (e.g., Tikhonov regularization) (*62*, *63*).

CW-ESR was in the past successfully used to measure distances in the 1−2 nm range (*29*). Recent advances in pulsed dipolar ESR spectroscopic (PDS) techniques have made it possible to measure large distances in doubly spin labeled biological macromolecules (*30*−*39*) and to determine oligomeric states of peptides (*40*, *41*) as well as soluble and membrane proteins in some cases (*38*, *42*). The PDS technique was most often applied to determine the dipolar couplings between two unpaired electron spins of the nitroxide spin labels introduced into the protein at specific locations (*32*, *33*, *36*, *38*, *42*), but in a few cases, it also used naturally occurring radicals (*43*−*46*). The electron dipolar coupling for a given electron spin separation, **r**, produces a characteristic oscillating time domain signal (Figure 1). The period of this oscillatory signal ($1/\nu_d$) exhibits an $\mathbf{r}^3$ dependence on the distance between the two coupled spins, and therefore, accurate distances in the range of 1−6 nm can be obtained from simple frequency measurements using available PDS techniques (*30*−*36*, *38*, *47*, *48*), and longer distances up to ∼8 nm can be evaluated for favorable conditions. Another advantage of PDS is that the same spin label can be placed in two (or sometimes more) different positions for which distance information is sought, as opposed to the fluorescence based techniques, wherein the donor label has to be distinguishable from the acceptor label. Using synthesized nitroxide spin labeled inhibitors or substrates, it is possible to specifically label the catalytic/binding sites of the protein of choice. This was performed in a few cases in different contexts unrelated to distance

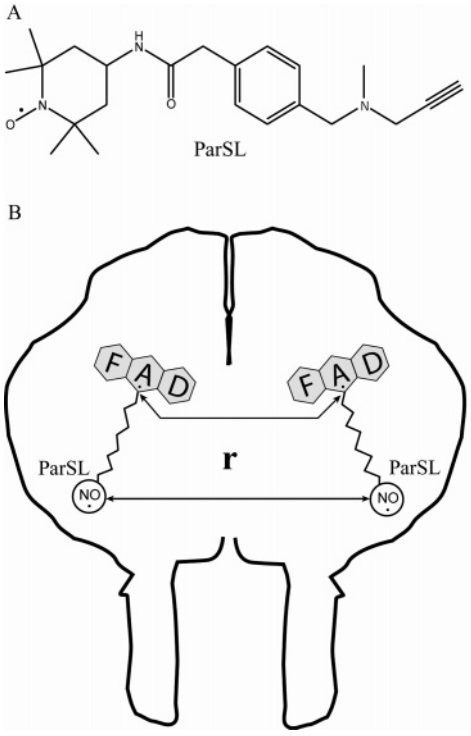

FIGURE 2: (A) Structure of the spin labeled inhibitor (ParSL) used in this study. (B) Schematics showing the spin labeling strategies used in this work. ParSL represents the spin labeled inhibitor used for spin labeling of each subunit of MAO in both the detergent solubilized and the OMM bound forms, and **r** denotes the interspin distances measured in this work. In one case, the distance is measured between the N5 centers of the flavin semiquione anion radical (upper arrow) and in the other, the distance connects two nitrogen atoms of the nitroxide groups of the ParSL spin probes (lower arrow).

measurements (*49*−*52*). When spin labeled substrates or inhibitors are specific for the protein of interest, chances of cross-labeling to other proteins in native biological environments are minimal and can be readily verified by control experiments. Therefore, the oligomeric form of a protein could be determined in its natural membrane environment, without requiring any detergent purification and reconstitution in artificial lipid bilayers or micelles. Under favorable conditions, quantitative information on the percentage of spins contributing to a unique distance can be determined by PDS, which would provide an estimate of the levels of dimerization (or oligomerization in general) in a biological system (*40*, *41*, *53*).

In this work, we used a synthetic spin labeled irreversible MAO inhibitor, named ParSL (Figure 2A), for covalently incorporating the nitroxide spin probe into the catalytic sites of human and rat MAOs in their OMM bound and detergent solubilized forms. The PDS technique used in this work was 4-pulse double electron−electron resonance (DEER) spectroscopy (*32*, *33*, *35*, *40*), known also as PELDOR, and was conducted at 17.35 GHz (Ku-band) to determine distances between the attached spin probes in the OMM bound and octyl β-D-glucopyranoside (OGP) purified MAOs. The OGP purified MAOs were further studied using one electron reduced anionic flavin semiquinone radical as the subunit specific endogenous spin probe at a different location in the protein (see Figure 2B for the schematics of the spin labeling strategies used in this work). The Glu-X to Lys or Lys-X to Glu mutants of human and rat MAOs in their OMM bound and OGP solubilized forms were also investigated to shed light on the significance of the human specific mutation. The interspin distances obtained by PDS studies were compared with those estimated from the available dimeric crystal structures of hMAOB (*10*, *11*) and rMAOA (*9*) (Figure 3A,B) to determine the oligomeric states and the proposed role of the conserved Glu-X residue in stabilizing the dimeric structures of MAOs (*12*). All human and rat MAOs were expressed in a *Pichia pastoris* expression system (*54*, *55*), and therefore, all OMM preparations have identical membrane environments. Similarly, all purified samples were prepared in OGP micelles following a uniform purification scheme (*55*) with minor modifications, thereby allowing comparative structural analyses under identical conditions.

The results of this investigation provide direct evidence for dimeric structures of all human and rat MAOs as well as their Lys/Glu mutants in the outer mitochondrial membrane, suggesting little or no role of the Glu-X residue in regulating MAO oligomerizations. The detergent solubilized human and rat MAOAs are observed to be partially dimeric (irrespective of Lys/Glu mutations), indicating a lower stability of the MAOA dimers in the OGP micelles as compared to the MAOB dimers.

MATERIALS AND METHODS

Expression of the Human and Rat Wild-Type and Mutant MAOs. Human MAOs were expressed in *P. pastoris* as reported previously (*54*, *55*). Wild-type rat MAOA and MAOB were expressed following similar protocols, which will be published elsewhere. The mutant enzymes were created using a Stratagene Quik-Change Site Directed Mutagenesis kit. The desired sequence alterations were confirmed by DNA sequence analysis and additional protein sequencing of the wild-type and mutant enzymes by in-gel trypsin (Promega) digestion and MALDI-TOF-MS (Bruker Ultraflex II TOF/TOF) of the liberated peptides.

Synthesis of Modified Pargyline Spin Label (ParSL). The nitroxide spin labeled pargyline (ParSL) inhibitor was synthesized following a protocol similar to that reported earlier for the synthesis of a pargyline based fluorescent MAO inhibitor (*56*). The fluorescent group used in the previous report was replaced with the 2,2,6,6-tetramethylpiperidine 1-oxyl (TEMPO) moiety to incorporate the nitroxide spin into the ParSL inhibitor. A detailed description of the ParSL synthesis is reported in our earlier work (*57*). The purified ParSL spin probe was characterized by ESI-MS (*m*/*z* peak at 371.25 Da for the $M + 1H^+$ ion), and purity was checked by TLC on a fluorescent coated silica gel 60 F_{254} plate (Merck).

Isolation of OMM. Intact mitochondria from *P. pastoris* KM71 cells expressing the wild-type and mutant human and rat MAOs were isolated by disrupting the cell wall using zymolyase (U.S. Biological) followed by sequential centrifugation steps in isotonic buffers as reported earlier (*58*). The OMMs were isolated from the intact mitochondria using osmotic shock and mild sonications followed by a 30−50% linear sucrose density gradient method, as reported earlier (*58*, *59*). OMM pellets were resuspended in 10 mM Tris-HCl buffer and used for the ParSL labeling immediately or were stored at −80 °C until further use.

Preparation of OMM Bound MAO Samples. The ParSL labeled OMM bound MAO samples were prepared by adding

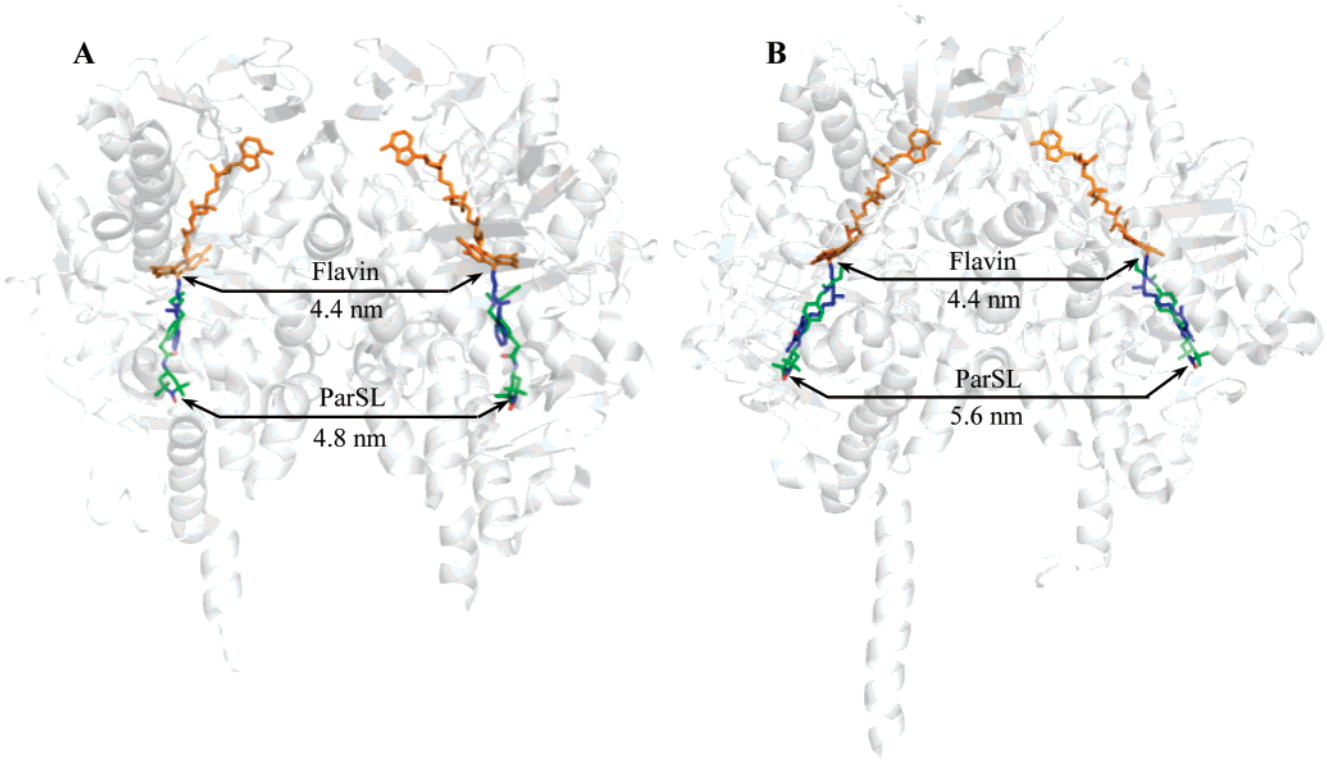

FIGURE 3: (A) Superimposed structure of the ParSL inhibitor into the hMAOB (PDB ID: IGOS) active site. The pargyline inhibitor originally present in the hMAOB X-ray structure is shown in blue. ParSL is shown with an atom color scheme of carbon: green, nitrogen: blue, and oxygen: red. The interspin distances based on the crystal structure for the flavin radicals (4.4 nm) and between the two nitroxide radicals of the ParSL inhibitors based on the superimposed structure (4.8 nm) are shown with arrows. (B) Structure of the ParSL inhibitor (shown with the same atom color scheme as in panel A) superimposed into the rMAOA (PDB ID: 1O5W) active site. Original inhibitor (clorgyline) present in the X-ray structure is shown in blue. Estimated interspin distances between the two flavin (4.4 nm) and ParSL spin probes (5.6 nm) are shown with arrows.

a 20−50-fold molar excess of ParSL to the samples and incubating at room temperature. The MAO concentrations in the OMM suspensions were estimated by comparing the units of activity per milliliter of membrane suspension with that of the corresponding purified enzyme of known concentration. The extent of inhibitor binding was monitored by the loss of catalytic activity over time. Complete inhibition was achieved within 1 h of incubation. The excess of free spin label was removed by repeated washings (3−4 times) with 60 mL of 10 mM Tris-HCl buffer, pH 7.4. The washed pellets were resuspended in 50 mM potassium phosphate in D_2O buffer, containing 10% (v/v) glycerol-d_8, pD 7.0.

Preparation of Detergent Solubilized Samples. Detergent (OGP) solubilized MAO samples were spin labeled by adding an ca. 50-fold molar excess of the spin labeled inhibitor (ParSL) and incubating at room temperature. The extent of spin labeling was determined by measuring the loss of enzyme activity over time. Excess spin label was removed by anion exchange chromatography using a Bio-Rad MacroPrep High-Q column (Bio Rad Laboratories) for MAOBs or DEAE Sepharose Fast Flow (Amersham Biosciences) column for MAOAs. The ParSL inhibited samples exhibited absorption peaks near 410 nm in the UV−vis spectra, indicating the formation of a flavocyanine adduct (*54*, *55*). Protein concentrations were determined by the biuret method.

Preparation of Flavin Radical Samples. Detergent (OGP) solubilized samples were deoxygenated under argon in a modified optical cell equipped with gastight fittings and then titrated with a solution of sodium dithionite of known concentration (standardized against a solution of riboflavin of known concentration). The generation of the anionic flavin semiquinone was monitored by UV−vis spectroscopy, following the appearance of its characteristic sharp absorption peak near 415 nm. The concentration of the flavin semiquinone radical was quantified from the decrease in absorbance at 450 nm ($\Delta\epsilon_{450} = 7.9\ mM^{-1}\ cm^{-1}$) upon reduction (*60*). The one electron reduced protein samples were transferred under argon atmosphere into 2.4 mm o.d. and 1.8 mm i.d. quartz sample tubes using a gastight syringe (Hamilton Inc.) and then frozen in liquid nitrogen for PDS measurements.

CW-ESR Spectroscopic Study. All ParSL inhibited detergent solubilized and OMM bound MAO samples were analyzed (data not shown) using a Bruker ESR-200D X-band (9.4 GHz) CW-ESR spectrometer equipped with a Bruker ST4102/8216 TE_{102} cavity at 25 °C to determine spin concentrations of labeled proteins and to assess the level of residual free (unbound) spin labels in the samples. At this temperature, the ESR spectra of free (unbound) spin labels have distinct narrow lines, which can be easily distinguished from the MAO active site-bound spin labels with spectral features typical of immobilized nitroxides. All ESR spectra were recorded using a 100 kHz modulation frequency and 0.2 mT modulation amplitude. Samples were loaded in quartz capillaries of 1.0 mm i.d. and 2.0 mm o.d. and placed in the standard 4 mm o.d. ESR sample tubes for spectral recordings. The spin concentration in each sample was determined by comparing the double integrals of the ESR spectra recorded on the ParSL inhibited MAO samples with that of a potassium nitrosodisulfonate (Sigma) spin standard of known

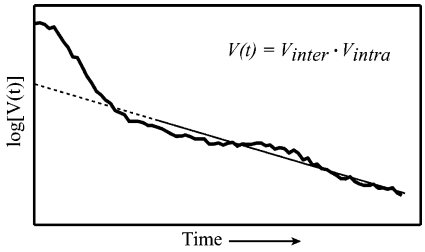

FIGURE 4: The signal $V(t)$ recorded in DEER spectroscopy must be corrected for the constant background contribution from V_{intra} (see text) and the monotonic decay due to V_{inter} before it can be used for extracting distance information from the frequency ν_d of the modulated part of V_{intra} [$V_{dip}(t)$, cf. Figure 1]. The background, modified with V_{inter}, is approximated by a low-order polynomial and subtracted from the original signal $V(t)$ to obtain the desired oscillating dipolar signal $V_{dip}(t)$. The solid line represents the fit to the later points of the experimental data and the dashed line shows an extrapolation to the earlier points to account for the temporal envelope of V_{inter}. The fit shown here is to straight line using a log scale, which is generally true for samples with uniform spin distributions.

concentration ($\epsilon_{545} = 20.8\ M^{-1}\ cm^{-1}$) (*61*). Only samples containing free spin label not exceeding 2% of the total spin concentration were used for PDS measurements.

OMM Sample Preparation for Distance Measurements. The sample preparation protocol in this case included 2−4 h of centrifugation of the spin labeled OMM suspensions loaded into 1.8 mm i.d. ESR sample tubes used in PDS measurements. The centrifugation was performed at 4 °C and 22 000*g*. The supernatant and excess sample were subsequently removed. The lipid-to-water ratios in the spun-down samples were checked gravimetrically in selected samples, and they were in the 1:6−1:8 range. The average spin concentrations were estimated from the amplitude of the primary echo, calibrated with 50% (w/v) water-glycerol solutions of stable nitroxide radical, 4-hydroxy-TEMPO, at a known concentration. Average spin concentrations in the samples were found to be in the range of ca. 50−150 μM. Local spin concentrations (i.e., in the membrane) were estimated from the slopes (i.e., k in the log plot in Figure 4) of the intermolecular contributions to the dipolar signals (vide infra), and they were consistent with the lipid-to-water ratios and average concentrations. Because of incomplete inhibitions and partial reductions of spin labels during sample preparation, the concentrations of the spin-coupled dimer (protein molecule with both subunits covalently labeled with a spin probe) were typically in the range of 15−70 μM (corresponding to 30−140 μM spin concentrations).

Distance Measurement by Ku-Band DEER. The primary (or refocused) electron spin echo amplitude recorded by DEER (*33*, *35*, *40*) is given by the product $V(t) = V_{inter}V_{intra}$ (cf. Figure 4). Here, $V_{intra}(t) = V_0\langle 1 - p(1 - \cos\ \omega(\mathbf{r})t)\rangle_{\mathbf{r}}$ contains the desired intramolecular dipolar signal, $V_{dip}(t) = pV_0\langle\cos\ \omega(\mathbf{r})t\rangle_{\mathbf{r}}$ from two dipole−dipole coupled electron spins on the same molecule (cf. Figure 1). Its amplitude is proportional to the fraction of spins at the pump frequency, $p \cong 0.1-0.3$ that are flipped by the pump pulse. Also, t (changing from 0 to t_m) is the dipolar evolution time in the respective pulse sequence, given by the properly referenced position of the pump pulse. Angular brackets denote averaging over all possible $\mathbf{r} \equiv (\mathbf{r},\theta)$ values. In an isotropic sample, $V_{dip}(t) = pV_0\langle\nu(\mathbf{r},t)\rangle_{\mathbf{r}}$, with $\upsilon(\mathbf{r},t) \equiv \int_0^1 du\ \cos[\gamma^2\hbar t(1 - 3u^2)/\mathbf{r}^3]$, where γ is the gyromagnetic ratio for the electron spin and $\hbar$ is the reduced Planck's constant. The remainder of V_{intra}, $V_0(1 - p)$, is the background from spins that input to the echo signal but have their partners unaffected by the pump pulse. V_{inter} represents the combined effect of (electron) spins that reside on all other molecules of the sample and is a monotonically decaying function of t. For a uniform distribution of molecules over the sample, it is a simple exponential decay with the exponent proportional to the spin concentration, C [i.e., $V_{inter} = \exp(-kCt)$]. Since all molecules beyond a certain distance add negligibly to the signal recorded over a finite time period (*47*), this concentration represents the local concentration. If the local spin distribution is not uniform (e.g., molecules reside in a lipid membrane), the decay is no longer simply exponential (*33*). V_{inter} and V_{intra} are usually normalized to unity at time zero; therefore, $V_{dip}(0)$ (or in other words, the modulation depth) is equal to the probability of spin flip by the pump pulse. Because the spin labeling efficiency, x, may be less than unity, the modulation depth is the product of the probability, p, of the spins being flipped by the pump pulse and x. Subtracting the background from the raw data leaves just the intramolecular dipolar signal $V_{dip}(t)$, which, in normalized form, is $xp\langle\cos\ \omega(\mathbf{r})t)\rangle_{\mathbf{r}}$. This dipolar signal is then analyzed by the Tikhonov regularization method (*62*), MEM (*63*), or other methods (*64*) to yield the interspin distance distribution, $P(\mathbf{r})$. [Note that V_{inter} cannot be analyzed in terms of $P(\mathbf{r})$ and must be removed by suitable methods.] The fwhm of this distribution depends on the flexibility of the spin label relative to the protein backbone and that of the protein itself. The distribution is a narrow-width peak for rigidly bound spin labels in distinct protein conformations. In the other limit of high flexibility, the distributions are broader, with the exception of some special cases (*32*, *37*, *65*).

Four-pulse DEER (*32*, *35*, *40*) experiments reported in this work were conducted using a home-built Ku-band (17.35 GHz) pulse FT-ESR/DQC spectrometer set to operate in the dual-amplifier DEER configuration. The probe-head was equipped with a dielectric resonator immersed into a CF935 helium flow cryostat (Oxford Instruments, Ltd.), as reported elsewhere (*32*). Sample temperatures were maintained in the range of 40−60 K, with the lower values used in the case of MAOBs. The pulse sequence used in the experiment is shown in Figure 5A. For the ParSL labeled samples, the pumping frequency was positioned at the center maximum of the ^{14}N nitroxide spectrum. The detection frequency, which was set at 65 MHz above the pumping frequency, corresponded to the low-field edge of the spectrum (Figure 5B). Similarly, for flavin radical samples, the pumping frequency was set on the high-field side of the center maximum, and the detection frequency was set 65 MHz above the pumping frequency toward the low-field edge of the spectrum (Figure 5C). The $\pi/2$ and π pulses of the 4-pulse DEER sequence were 16 and 32 ns, respectively, for the detection mode, (which uses the $\pi/2-\pi-\pi$ refocused primary echo pulse sequence). The pump π pulse width was 20 ns. Because of large distances between the ParSL labels in MAO, it was necessary to acquire signals over a time period (t_m) of 4−5 μs. The signal decay due to phase relaxation resulted in echo amplitudes for such times reduced by a factor of 30−100 as compared to their reference amplitudes measured by using the primary echo sequence with a 0.25 μs pulse separation and the same widths of $\pi/2$ and π pulses as used in DEER.

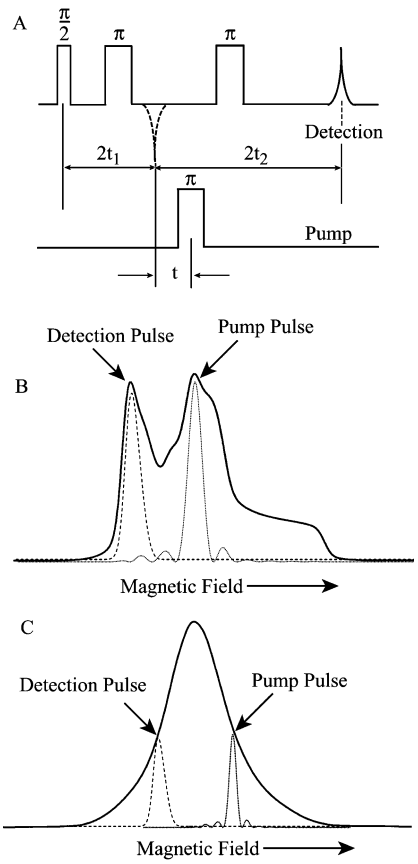

FIGURE 5: (A) Schematics of the four-pulse DEER pulse sequence used in this work. Positions of the pump (dotted line) and detection (dashed line) pulses in the integrated ESR spectra of the ParSL and flavin semiquinone anion radical are shown in panels B and C, respectively.

Phase relaxation times were in the range of 1.7−2.2 μs (some increase in this range was observed for MAOA samples by using the deuterated buffer), with the upper value corresponding to MAOA in OGP. Nevertheless, despite these challenges, a good SNR of 50−100 was obtained after 12−24 h of signal averaging at a 1−2 kHz pulse repetition rate. The flavin radical posed a challenge due its long spin− lattice relaxation time, t_1. Therefore, data collections were conducted at 100 K at a 200 Hz pulse repetition rate, and signal recording was usually limited by a t_m value of 2.5 μs.

Spin Counting. The intramolecular part of the DEER signal $V_{intra}(t) = V_0\langle 1 - p(1 - \cos \omega(\mathbf{r})t)\rangle_{\mathbf{r}}$ contains the dipolar signal $V_{dip}(t) = pV_0\langle \cos \omega(\mathbf{r})t\rangle_{\mathbf{r}}$ originating from (nitroxide or flavin radical) electron spin pairs on each of the labeled molecules (*33*) (cf. Figure 2). (We are assuming here that $x = 1$.) If there are more than two electron spins within a localized group (e.g., an oligomer), it follows that $V_{intra} = \langle\langle \prod_{k\neq i}^{N}[1 - p(1 - \cos \omega(\mathbf{r}_i - \mathbf{r}_k)t]\rangle\rangle_{\mathbf{r}_k,\mathbf{r}_i}$, where angle brackets represent the averaging over all possible spatial configurations of spins in the group. This gives rise to an increase in modulation depth of V_{intra} by a factor of $\sim(N - 1)$, where N is the number of spins in the group (or oligomer) (*53*, *66*). Therefore, spin counting amounts to measuring this modulation depth, $\approx p(N - 1)$ (for small p) at asymptotic conditions (i.e., when the oscillating terms $\cos[\omega_{ik}(\mathbf{r}_i - \mathbf{r}_k)t]$ average to zero at sufficiently large times, t). If the maximum time available for signal recording with acceptable SNR is t_m, then if in the cluster all distances, $\mathbf{r}$ values are less than $R \approx (\gamma^2\hbar t_m/2\pi)^{1/3}$, the asymptotic behavior can be reached. This condition is implicit in spin counting by DEER. It is essential that p should be obtained by calibration using a sample of a nitroxide biradical (or doubly labeled peptide) with x close to unity, or else an error may result. Gramicidin-A (GA-sl), spin labeled at its C-terminus and incorporated into lipid membrane multi-bilayer vesicles of dimyristoylphosphatidylcholine (DMPC) in a ratio of 1:1,000, was used for this purpose as a reference for the spectral excitation. GA-sl is known to be dimeric in phospholipid membranes of DMPC (*48*). GA-sl was at least 99% pure as verified by mass spectroscopy. The samples were very stable over time, and no free spin label was detected by CW-ESR. GA-sl reference samples consistently yielded normalized dipolar signals within 5% of theoretical values of p expected for uniform B_1 values and uncorrelated magnetic tensors [i.e., they were close to a value of 0.31, as expected for the pulse sequence used (cf. previous section)]. The calibration results are equally applicable to data from membrane bound and detergent purified MAO samples studied using the same pulse widths and power setting. Maintaining reproducible conditions over the course of experiments was facilitated by our dual-amplifier spectrometer configuration and the stability of the resonator tuning.

Spins at short distances (<2 nm) fall outside the DEER range and will have their signal (and consequently the value of N) attenuated. Also, it is assumed that the spins are like spins with very similar values of their phase relaxation times, and there are no angular correlations of the anisotropic parts of the respective magnetic tensors. When these assumptions are not the case, the estimate for N would be smaller. It will also be reduced by incomplete spin labeling or the presence of a free spin label. In model studies (*53*), it has been found that sometimes N was not an integer number. Given these factors, rounding off to a higher integer would give a better estimate. In this work, the main source of error was caused by incomplete spin labeling, which was addressed as described earlier in this section. For a t_m value of 4−5 μs, used in this work, R is 6.0−6.5 nm; therefore, MAO dimers and small oligomers (with N values of 3 or 4, depending on geometry) are expected to fall within the spin counting limiting conditions. Oligomers of size greater than R could lead to an underestimation of N.

Estimation of Interspin Distances from the Dimeric X-ray Structures of hMAOB and rMAOA. To determine the oligomeric states of MAOs in detergent purified and OMM bound forms, the interspin distances measured by the PDS technique were compared to those estimated from the dimeric crystal structures of hMAOB (PDB ID: 1GOS) and rMAOA (PDB ID: 1O5W). For the detergent purified flavin radical samples, interspin distances obtained from PDS measurements were directly compared to those determined by measuring the distances between the flavin N5 centers (see Figure 3A,B and Table 1), providing adequate accuracy for this distance. Since no crystal structure is available for ParSL inhibited MAOs, the interspin distances in these samples were estimated by superimposing the ParSL spin probe in the crystal structures of hMAOB and rMAOA. The superimposed structures (Figure 3A,B) were generated using program O version 7.0.1 (*67*). The energy minimized coordinates of different rotamers of the ParSL molecule were first generated by CS Chem3D Pro 5.0 (Cambridge Software

Table 1: Interspin Distances from the PDS Study and the Corresponding Distances from X-ray Crystallography

	PDS distances (nm)			estimated distances[a] (nm)	
	OMM	detergent			
samples	ParSL	ParSL	flavin	ParSL	flavin
hMAOB	4.7 ± 0.1	4.7 ± 0.1	4.3 ± 0.1	4.8	4.4
hMAOB-E-142-K	4.7 ± 0.1	4.7 ± 0.1	4.2 ± 0.1	N/A	N/A
rMAOB	4.9 ± 0.1	4.9 ± 0.1	4.2 ± 0.1	N/A	N/A
rMAOA	5.6 ± 0.3	6.2 ± 0.3	4.3 ± 0.1	5.6	4.4
hMAOA	5.6 ± 0.3	5.7 ± 0.3	4.2 ± 0.1	N/A	N/A
hMAOA-K-151-E	5.6 ± 0.3	5.9 ± 0.3	4.3 ± 0.1	N/A	N/A

[a] Distances estimated from the X-ray structures of hMAOB (PDB ID: 1GOS) and rMAOA (PDB ID: 1O5W).

Corp.) software and saved as PDB files. The energy optimized ParSL rotamers were then manually superimposed with the inhibitors (clorgyline in rMAOA and pargyline in hMAOB) originally present in the X-ray structures. The spatial orientation of the ParSL inhibitor was adjusted as required to minimize the side chain interactions and to maximize the overlap with the existing inhibitor. The rotamer showing minimal unfavorable interactions with the protein side chains, and maximal overlap with the existing inhibitors were used for generating the superimposed structures. The interspin distances estimated from the ParSL superimposed on hMAOB and rMAOA are shown in Figure 3A,B, respectively. The distances obtained by PDS measurements on human and rat MAOs were compared with these distances to determine their oligomeric states in the detergent purified and OMM bound forms. All structures shown in this article were rendered using PyMol v.99 molecular graphics software (http://www.pymol.org).

RESULTS

Distance Measurements on ParSL Inhibited OMM Bound Wild-Type Human and Rat MAOB Samples. The PDS data for ParSL labeled wild-type hMAOB (solid line) and rMAOB (dashed line) in OMM are shown in Figure 6A. The dipolar signals for the two enzymes look quite similar. The inset in Figure 6A shows the corresponding distance distributions obtained by inverse reconstruction based on the L-curve Tikhonov regularization (*62*), further refined by MEM (*63*). The average interspin distance obtained for hMAOB (4.7 ± 0.1 nm) is within the uncertainty of the distance (4.8 nm) estimated from the ParSL superimposed structure of hMAOB (Figure 3A), and that for rMAOB (4.9 ± 0.1 nm) is very close. It is worth mentioning here that the crystal structure of rMAOB is not known. The similarities in the interspin distances and dipolar signal amplitudes (modulation depths) indicate that both hMAOB and rMAOB are indeed dimeric in OMM. The non-reproducible peaks of small volume (indicated with arrows) visible in the distance distributions are due to artifacts of baseline subtraction, non-zero effects of magnetic tensors correlations (*40*) in the case of MAOBs, and limitations of distance distribution reconstruction methods (cf. Material and Methods). The positions and intensities of these spurious peaks varied for different analyses and cannot be attributed to a true dipolar distance. The distance distributions for ParSL labeled human and rat MAOB samples are very distinct with a fwhm of ca. 0.7 nm. This demonstrates that ParSL has a limited flexibility in its binding

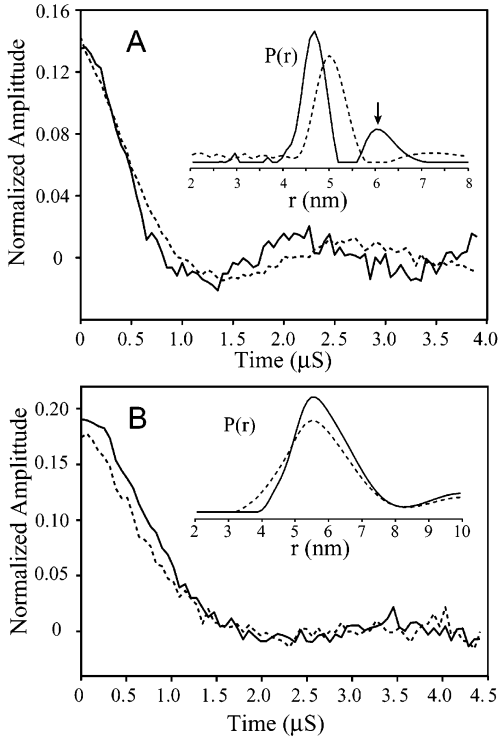

FIGURE 6: (A) PDS data for ParSL inhibited wild-type hMAOB (solid line) and rMAOB (dashed line) in the OMM. (B) PDS data for ParSL inhibited hMAOA (solid line) and rMAOA (dashed line) in the OMM. The insets show the respective distance distributions. The average concentrations of the doubly labeled protein were ca. 25 μM (hMAOB), 70 μM (rMAOB), and 35−40 μM (human and rat MAOAs).

sites in human and rat MAOB, as opposed to the case of human and rat MAOAs (vide infra).

Distance Measurements on ParSL Inhibited OMM Bound Wild-Type Human and Rat MAOA Samples. Figure 6B shows the PDS data obtained on ParSL labeled wild-type hMAOA (solid line) and rMAOA (dashed line). If the Glu-151 residue is important in stabilizing the dimeric structure of MAOA, as implicated in previous studies (*12*), only rMAOA should yield a dipolar signal, whereas hMAOA should exhibit a monotonically decaying signal that is slightly convex on a logarithmic scale, as is typical in the case of monomers uniformly distributed on a surface. (At a high lipid content in OMM samples, the intermolecular contribution, V_{inter}, was an intermediate of 2-D and 3-D cases, pointing to a significant fraction of closely spaced membrane bilayers). The dipolar signal obtained from the ParSL labeled hMAOA sample appears to be nearly identical to that obtained for rMAOA in their respective OMM bound forms. Both samples show an average interspin distance of 5.6 ± 0.3 nm (inset Figure 6B and Table 1). These distances are in good agreement with that estimated (5.6 nm) by superimposing the ParSL inhibitor in the rMAOA crystal structure (Figure 3B), demonstrating that hMAOA as well as rMAOA are dimeric in OMM.

An alternative explanation for observing the spin pair-like dipolar signal from the ParSL bound hMAOA sample could be its high level of expression in *P. pastoris*, leading to relatively high local (lateral) concentration within the OMM lipid bilayer. To test this possibility, PDS measurements on OMM bound hMAOA and rMAOA were performed at various expression levels. The total MAO-to-

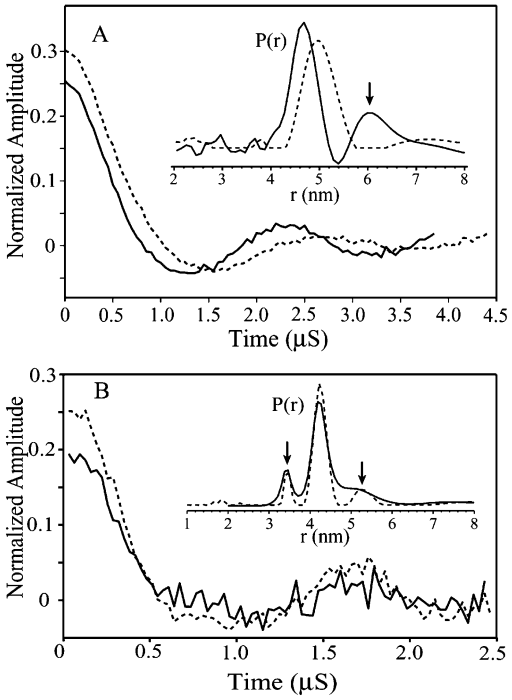

FIGURE 7: (A) PDS data for ParSL inhibited wild-type hMAOB (solid line) and rMAOB (dashed line) in OGP micelles. (B) PDS data for the flavin radical samples of wild-type hMAOB (solid line) and rMAOB (dashed line) in OGP micelles. Distance distributions are shown in the insets.

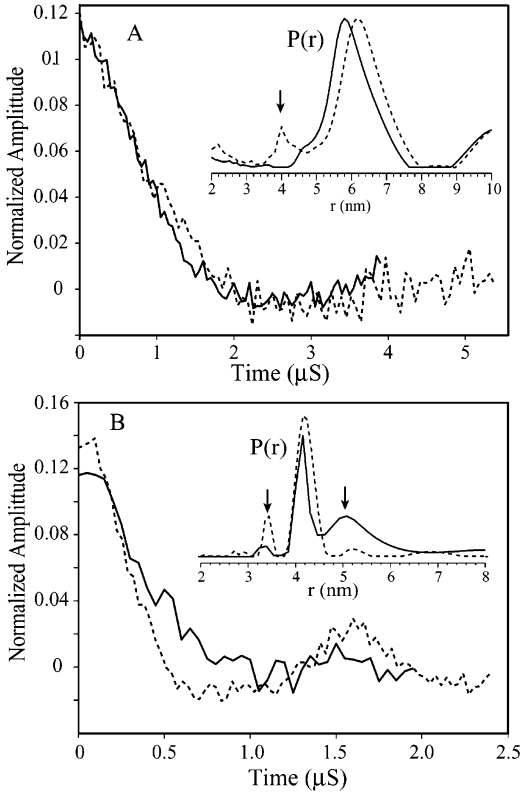

FIGURE 8: (A) PDS data for ParSL inhibited wild-type hMAOA (solid line) and rMAOA (dashed line) in OGP micelles. Inset shows the corresponding distance distributions. (B) PDS data for the flavin radical samples of wild-type hMAOA (solid line) and rMAOA (dashed line) in detergent micelles. The inset shows the distances obtained for hMAOA (solid line) and rMAOA (dashed line) flavin samples.

protein ratio in the OMM was varied by almost a factor of 3 for each sample. The dipolar signals from these samples were independent of the level of expression (not shown). These data support the conclusion that both hMAOA and rMAOA are dimeric in the OMM, which contradicts the previous hypothesis proposing a monomeric form for hMAOA. Therefore, the X-ray crystallographic structure of hMAOA does not reflect its physiological oligomeric state in the OMM.

Distance Measurements on Wild-Type Human and Rat MAOB Samples in Detergent (OGP) Solubilized Forms. The baseline subtracted PDS data on the detergent solubilized ParSL labeled wild-type human (solid line) and rat (dashed line) MAOB are shown in Figure 7A. The inset in Figure 7A shows the interspin distance distributions obtained for the two samples. The average interspin distances for the detergent purified human and rat MAOB samples agree very well with those obtained for the corresponding OMM bound samples (cf. the inset in Figure 6A and Table 1).

Figure 7B shows the PDS data obtained on detergent solubilized human and rat MAOBs using endogenous anionic flavin semiquinone radicals as spin labels, generated by reduction with dithionite (see Materials and Methods). The interspin distances of ca. 4.3 ± 0.1 nm were obtained in this case (see the inset in Figure 7B and Table 1) and are in very good agreement with that estimated from the known crystal structure of hMAOB (see Figure 3A). These data further confirm that human and rat MAOB retain their dimeric structures in their respective detergent solubilized forms. Furthermore, the similarities in the distances obtained in detergent solubilized and OMM bound forms with those estimated from the known crystal structure of hMAOB show that the structures of human and rat MAOB in OGP detergent micelles remain largely unaltered after all the extraction and purification steps. Small spurious peaks around 3.5 and 5.5 nm in the distance distribution plot of the flavin samples (indicated by arrows in the inset of Figure 7B) in part may be due to reconstruction artifacts caused by unavoidable errors in baseline subtraction, but more likely, they are due to nuclear ESEEM (electron-spin echo envelope modulation) effects (*30, 40*) and angular correlations of magnetic tensors of confined flavin radicals and should be ignored. The regularization methods used to reconstruct distance distributions attempt to account for such small artifacts by generating extraneous peaks, which are clearly recognizable as such due to their typically irreproducible amplitudes and positions. But, they tend to appear at the same positions in cases of small consistent signal modulation (e.g., caused by ESEEM or to a lesser extent by correlations of magnetic tensors).

Distance Measurements on Wild-Type Human and Rat MAOA Samples in Detergent Solubilized Forms. Figure 8A shows the PDS data obtained on ParSL labeled human (solid line) and rat (dashed line) MAOAs solubilized in OGP. The inset in Figure 8A shows reconstructions of the distance distributions for the hMAOA and rMAOA samples. Average distances (Table 1) are (within error) the same as obtained for the corresponding OMM samples (Figure 6B). Normalized dipolar signal intensities for detergent solubilized human and rat MAOA are about 40−50% of those observed in their OMM bound forms. Given that spin labeling efficiencies were nearly equal in both cases, this indicates that human and rat MAOA dimers are less stable in OGP micelles as compared to those of human and rat MAOBs.

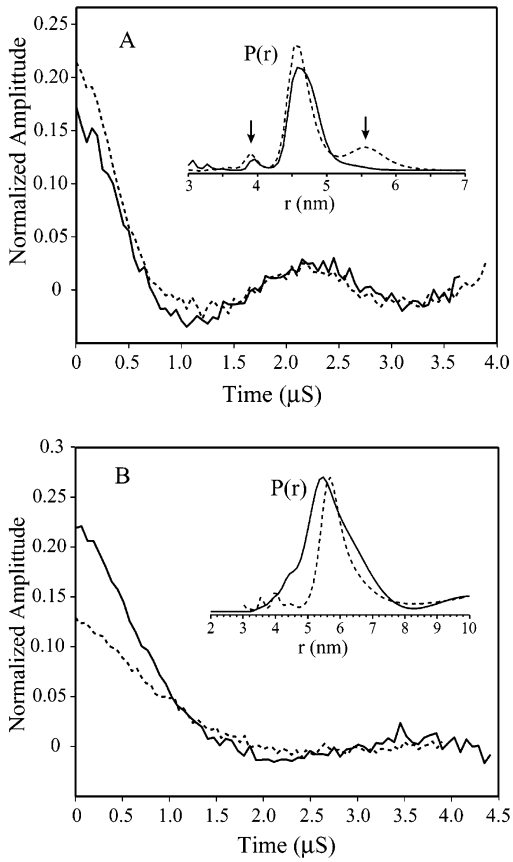

FIGURE 9: (A) PDS data for the ParSL inhibited hMAOB-Glu-142-Lys mutant in the OMM bound (solid line) and in the detergent (OGP) micelles (dashed lines). (B) PDS data for ParSL inhibited hMAOA-Lys-151-Glu mutant in the OMM (solid line) and detergent (dashed line). The inset demonstrates respective distance distributions.

The PDS data obtained on human and rat MAOAs using the endogenous flavin semiquinone radical as the spin probe are shown in Figure 8B. The inset shows distance distributions obtained for these samples with the measured interspin distances listed in Table 1. As with the ParSL labeled samples shown in Figure 8A, the flavin radical samples of human and rat MAOAs also show that only about 50% of the species is present in the dimeric form.

Role of the Conserved Glu-X Residue in Regulating MAO Dimeric Structures. The pulsed ESR data discussed previously suggest no role of the conserved Glu-X residue in stabilizing the dimeric structures of human and rat MAOs in their OMM bound and detergent solubilized forms. To further confirm this conclusion, we created the Lys-151-Glu mutant of hMAOA with the goal of stabilizing the dimer. In addition, the Glu-142-Lys mutant of hMAOB was constructed with the intention of testing as to whether that substitution aids dissociation of the dimer. The background-corrected PDS data on the ParSL labeled Glu-142-Lys mutant of hMAOB in the detergent solubilized (dashed line) and OMM bound (solid line) forms are shown in Figure 9A. Corresponding interspin distance distributions are shown in the inset. The average distances are summarized in Table 1. As is evident from the data, mutation of the conserved Glu-142 residue to Lys in hMAOB shows no measurable effect on the observed interspin distances and the dimerization state of hMAOB in its detergent solubilized and OMM bound forms. PDS data with the flavin radical as the spin probe (not shown) on this mutant enzyme also show a dimeric structure, with the inter-flavin distance being identical to that observed for the wild-type enzyme (Table 1). PDS data on the ParSL labeled Lys-151-Glu mutant of hMAOA are shown in Figure 9B for detergent solubilized (dashed line) and OMM bound (solid line) forms. The inset shows the corresponding interspin distance distributions, with the average distances summarized in Table 1. As explained previously for wild-type hMAOA, the mutant enzyme remains dimeric in the OMM bound form. In the detergent solubilized form, the Lys-151-Glu mutant of hMAOA behaves similarly to the wild-type, showing a signal corresponding to the presence of ca. 50% dimeric species. These data, taken together with the hMAOB-Glu-142-Lys mutant data, confirm no role of the conserved Glu-X (X being 151 in MAOAs and 142 in MAOBs) residue in stabilizing the dimeric structures of either enzyme.

DISCUSSION

Recent advances in our understanding of the properties of biological membranes have revealed several aspects of protein−lipid interactions, which are important in stabilizing the oligomeric structures of membrane proteins (*25*, *26*, *68*). Dimerization has been observed to be a common motif for many membrane proteins (e.g., cytochrome *b*6f, rhodopsin, etc.) in regulating their stabilities and functions (*24*, *25*, *69*, *70*). Since structural and functional properties of membrane proteins are sensitive to extraction and purification in detergent micelles, an ongoing quest is to understand their oligomeric states in natural membrane bound forms. The results presented above with human and rat MAOs illustrate the applicability of a PDS based technique (DEER) toward achieving this goal. To our knowledge, this is the first study reporting on probing oligomeric states of membrane proteins in their natural biological membrane environments using a PDS based technique. Parallel studies shown here with the detergent solubilized forms of these enzymes (human and rat MAOs) by using the same active site specific spin label (ParSL) and additionally the endogenous flavin semiquinone radicals enabled us to perform the comparative analyses of the structural properties of these enzymes in their detergent solubilized and OMM bound forms.

Correlation of the PDS Data with the Available X-ray Structures of MAOs: Determination of Oligomeric States. The interspin distances (Table 1) between two active-site bound ParSL inhibitors, or endogenously created anionic flavin semiquinone radicals, have been used as spectroscopic signatures to identify oligomeric states of human and rat MAOs in their OMM bound and detergent solubilized forms (see Figure 2). The distances determined from dipolar couplings of the radical species in human and rat MAOs show good agreement with those derived from the available dimeric X-ray structures of hMAOB and rMAOA (Figure 3A,B and Table 1). It can therefore be reasonably concluded that the quaternary structures of human MAOB and rat MAOA in their OMM bound forms are close to those derived from X-ray structural analysis in their respective purified forms. To the best of our knowledge, this level of agreement between PDS and X-ray structural data on membrane bound enzymes has not been demonstrated in any previous study. The direct correlation between the inter-flavin radical

distances estimated from X-ray structures with those measured by PDS show that the quaternary structures of hMAOB and rMAOA are the same in their inhibited and uninhibited forms. This information is of importance since only the inhibited forms of the enzymes are amenable to crystallization and subsequent X-ray structural analysis. Allosteric regulation of protein oligomerization has been reported for carbamoyl phosphate synthase from *Escherichia coli* (*71*). The current PDS data thus suggest that the dimeric structures of MAOs in detergent micelles are not influenced by the binding of covalent inhibitors.

Presence of Higher Oligomeric Species in OMM and OGP Micelles. One important application of the PDS based techniques is that the average number of spins per protein (or peptide) oligomers can be determined from the modulation depth of dipolar signals (cf. Materials and Methods). The outcome of spin counting is, however, sensitive to the spin labeling efficiency and also to the presence of free spin labels with a long phase memory time, t_m (i.e., exposed to or in the aqueous phase), which necessitated careful removal of unreacted spin label. Polydispersity due to the presence of loosely held higher oligomers in the sample complicate matters further since for such a system (dimer of dimers, pentamer, etc.), N would be difficult to estimate as the asymptotic signal behavior may not necessarily be attained. These situations were addressed by carefully removing the excess free spin label from the samples used for PDS measurements and by performing PDS measurements on the ParSL labeled detergent purified and OMM bound MAOA samples at varying concentrations. No concentration dependences of modulation depth and signal shape were observed. This indicates that higher oligomers were not present in significant amounts in the MAOA samples tested in this work. Furthermore, the possibility of the presence of higher oligomers (trimers or tetramers) with interspin distances comparable to those of a true dimer can also be ruled out. First, we note that the size of the protein permits at least three spin labels to be in a conceivable construct within a distance of 6.5 nm, which is the asymptotic limit for the dipolar signal on the time-scale, t_m, used. In this case, the dipolar signal would be expected to increase by about a factor of $\sim 2-3$, as compared to that from the GA-sl reference (depending on proximities of other spins in, e.g., a tetramer). However, the only values that we obtained were ≤ 0.5 that of the reference.

It should be noted, however, that the PDS data presented here cannot completely rule out the presence of loosely held higher oligomers with interspin distances significantly greater than 6.0 nm. For such oligomers, dipolar coupling between the electron spins would not noticeably modify the oscillatory dipolar signals (V_{intra}) that generate the $P(\mathbf{r})$ values but would add to the baseline signal considered as V_{inter} and thus remain unseen in our measurements. This scenario is rather unlikely for the OMM bound forms due to the constraints of residing in the membrane.

Percentage of Dimeric Species in OMM and OGP Micelles. Since the dipolar signals presented in this work originate mainly from dimers, the information on the modulation depths can be used to estimate the percentage of dimeric species in the sample (i.e., the monomer-to-dimer ratio) (*42*). However, PDS signals in biological samples are often affected by spin labeling efficiency as we have already discussed and by the presence of small amounts of free spin labels in the samples. Incomplete spin labeling will directly affect the estimate of the monomer-to-dimer ratio. This error could be reduced in this work by determining MAO-to-spin concentration ratios for each sample (cf. Materials and Methods). In OGP micelles, the maximum p value (fraction of the spins flipped by the pump pulse) of the ParSL labeled human and rat MAOA samples was about 50% of that observed for the corresponding MAOB samples. The same ratio of $\sim$50% was also observed for the flavin radical samples of MAOAs as compared to MAOBs, where the issue of free spin labels does not exist and interspin distances are much shorter (4.4 nm) with a well-defined signal oscillation (Figure 8B), whereas, in the OMM bound form, ParSL labeled MAOAs and MAOBs had nearly identical p values.

Analyses of the modulation depths of the dipolar signals from all the OMM bound and detergent solubilized human and rat MAOB samples indicate the presence $\sim$100% dimeric species after typical spin labeling efficiencies ($\sim 60-70\%$ for OMM bound and $\sim$90% for detergent purified samples) are accounted for (cf. Materials and Methods). This observation is consistent with the 100% dimeric species observed in previous hydrodynamic studies on hMAOB solubilized in Zwittergent 3-12 detergent micelles (*8*), as well as with all the X-ray structures reported for hMAOB with different reversible and irreversible inhibitors (*10*, *11*, *72*, *73*). Rat MAOB, for which no such hydrodynamic or X-ray structural studies have been reported, also shows a uniform dimeric structure in the detergent solubilized and OMM bound forms. These data thus indicate that the dimeric structures of human and rat MAOBs are quite stable to detergent extractions and purifications.

Similar analyses of the PDS data on ParSL labeled human and rat MAOAs show nearly 100% dimeric species in the OMM. However, in the OGP solubilized forms, both of these two enzymes reproducibly show no more than 50% dimeric species. It is worth mentioning that some uncertainty in this result may originate from small amounts ($\sim$1%) of residual free spin label, whose long relaxation time, as compared to the protein active site bound ParSL, could increase its contribution to the background by a factor of up to $30-50$ in detergent based samples (with the upper range reflecting the shorter t_m values of MAOBs), as can be estimated assuming that free label t_m is in the range of $4-6\ \mu$s, featured by water-exposed nitroxides (*40*) and using typical t_m values. However, consistent results have also been observed for these enzymes in OGP micelles with anionic flavin semiquinone radicals as the spin probes, where the free spin label issue does not exist and the spin labeling efficiency is accurately estimated by optical measurements. The data on faster relaxing MAOB in OGP, where it is exclusively dimeric, also indicated that any free label contribution was suppressed. The data thus show that the dimeric structures of human and rat MAOAs partially dissociate in the OGP micelles. Our effort to determine the equilibrium dissociation constant by varying the sample concentrations was unsuccessful, partly due to the difficulty of using the flavin semiquinone radical as the PDS spin probe (cf. Materials and Methods).

These data partly agree with the results obtained from the hydrodynamic studies (*8*) on hMAOA, showing ca. 40% monomeric (65 kDa) and 60% higher oligomeric (330 kDa) species (loose aggregates of dimers and monomers) in OGP

micelles. Such aggregates may show signals close to those of dimers in the OGP micelles, as discussed previously. However, it should also be noted that the buffers used in previous hydrodynamic studies (*8*) on hMAOA contained no glycerol, which has been observed to be essential for the stability of the purified protein. In the case of rMAOA, no hydrodynamic study in OGP micelles has been reported. The X-ray structure of rMAOA was determined using *N*-dodecylphosphocholine (FOS-Choline 12) as the detergent (*9*), which has different properties than the OGP micelles used in this study. Therefore, the partial dissociation observed for human and rat MAOA structures in OGP micelles is a detergent dependent effect and does not reflect their true oligomeric states in the OMM. Presumably, hMAOA is more amenable to form crystals in the monomeric state than in the dimeric state, resulting in the observed monomeric X-ray structure in the OGP micelles (*8*).

Role of the Conserved Glu-X Residue in Stabilizing MAO Dimers. The PDS results presented previously with the Lys-151-Glu mutant of hMAOA and Glu-142-Lys mutant of hMAOB clearly demonstrate that the conserved Glu-X (with X being 151 in MAOAs and 142 in MAOBs) residue plays no significant role in stabilizing the dimeric structures of human and rat MAOs, in contrast to the hypothesis proposed by Andrés et al. based on sequence analyses and modeling studies (*12*). The present data did show, however, that human and rat MAOA dimers are considerably less stable in OGP micelles as compared to MAOBs.

CONCLUSION

The PDS data presented previously show that the conserved Glu-X residue in human and rat MAOs does not represent an essential mechanism of regulating oligomeric state of the enzyme in the OGP solubilized or OMM bound forms, contrary to a previous hypothesis (*12*). Therefore, the observed difference between the oligomeric states of hMAOA in the X-ray structure and in the OMM is likely due to the dissociation of its dimeric structure during purification and crystallization in the OGP micelles (the detergent used for X-ray crystallization of hMAOA) (*8*). This is consistent with the observation of only an ~50% dimer-like structure in the OGP solubilized hMAOA and hMAOA-Lys-151-Glu samples.

Two major conclusions can be drawn from the PDS data presented in this study. The first is that the direct correlation between the interspin distances measured on OMM bound hMAOB and rMAOA samples with the corresponding crystallographic distances indicate that their structures in OMM bound forms agree with that reported in X-ray studies. The second conclusion is that the difference observed between the oligomeric states of hMAOA in the OMM and that reported by the X-ray crystallographic study indicates that OGP is not an efficient membrane mimetic for hMAOA. The results presented here clearly demonstrate the utility of PDS based studies, using a protein specific spin labeled inhibitor, in elucidating oligomeric states and structural properties of membrane proteins in their natural membrane environment.

ACKNOWLEDGMENT

The authors are thankful to Boris Dzikovski for the spin labeled gramicidin-A sample and useful discussions. The authors also thank Milagros Aldeco for her help in obtaining purified human MAOA and MAOB enzymes.

REFERENCES

1. Silverman, R. B. (1995) Radical ideas about monoamine oxidase, *Acc. Chem. Res. 28*, 335−342.
2. Youdim, M. B. H., Edmondson, D., and Tipton, K. F. (2006) The therapeutic potential of monoamine oxidase inhibitors, *Nat. Rev. Neurosci. 7*, 295−309.
3. Cases, O., Seif, I., Grimsby, J., Gaspar, P., Chen, K., Pournin, S., Muller, U., Aguet, M., Babinet, C., and Shih, J. C. (1995) Aggressive behavior and altered amounts of brain serotonin and norepinephrine in mice lacking MAOA, *Science (Washington, DC, U.S.) 268*, 1763−1766.
4. Brunner, H. G., Nelen, M., Breakefield, X. O., Ropers, H. H., and van Oost, B. A. (1993) Abnormal behavior associated with a point mutation in the structural gene for monoamine oxidase A, *Science (Washington, DC, U.S.) 262*, 578−580.
5. Shih, J. C., Chen, K., and Ridd, M. J. (1999) Monoamine oxidase: From genes to behavior, *Ann. Rev. Neurosci. 22*, 197−217.
6. Holschneider, D. P., Chen, K., Seif, I., and Shih, J. C. (2001) Biochemical, behavioral, physiologic, and neurodevelopmental changes in mice deficient in monoamine oxidase A or B, *Brain Res. Bull. 56*, 453−462.
7. Shih, J. C., and Thompson, R. F. (1999) Monoamine oxidase in neuropsychiatry and behavior, *Am. J. Hum. Genet. 65*, 593−598.
8. De Colibus, L., Li, M., Binda, C., Lustig, A., Edmondson, D. E., and Mattevi, A. (2005) Three-dimensional structure of human monoamine oxidase A (MAO A): Relation to the structures of rat MAO A and human MAO B, *Proc. Natl. Acad. Sci. U.S.A. 102*, 12684−12689.
9. Ma, J., Yoshimura, M., Yamashita, E., Nakagawa, A., Ito, A., and Tsukihara, T. (2004) Structure of rat monoamine oxidase A and its specific recognitions for substrates and inhibitors, *J. Mol. Biol. 338*, 103−114.
10. Binda, C., Li, M., Hubalek, F., Restelli, N., Edmondson, D. E., and Mattevi, A. (2003) Insights into the mode of inhibition of human mitochondrial monoamine oxidase B from high-resolution crystal structures, *Proc. Natl. Acad. Sci. U.S.A. 100*, 9750−9755.
11. Binda, C., Newton-Vinson, P., Hubalek, F., Edmondson, D. E., and Mattevi, A. (2002) Structure of human monoamine oxidase B, a drug target for the treatment of neurological disorders, *Nat. Struct. Biol. 9*, 22−26.
12. Andrés, A. M., Soldevila, M., Navarro, A., Kidd, K. K., Oliva, B., and Bertranpetit, J. (2004) Positive selection in MAOA gene is human exclusive: Determination of the putative amino acid change selected in the human lineage, *Hum. Genet. 115*, 377−386.
13. Krueger-Koplin, R. D., Sorgen Paul, L., Krueger-Koplin, S. T., Rivera-Torres, I. O., Cahill, S. M., Hicks, D. B., Grinius, L., Krulwich, T. A., and Girvin, M. E. (2004) An evaluation of detergents for NMR structural studies of membrane proteins, *J. Biomol. NMR 28*, 43−57.
14. Kunji, E. R. S. (2004) The role and structure of mitochondrial carriers, *FEBS Lett. 564*, 239−244.
15. Pebay-Peyroula, E., Dahout-Gonzalez, C., Kahn, R., Trezeguet, V., Lauquin, G. J. M., and Brandolin, G. (2003) Structure of mitochondrial ADP/ATP carrier in complex with carboxyatractyloside, *Nature (London, U.K.) 426*, 39−44.
16. Kunji, E. R. S., and Harding, M. (2003) Projection structure of the atractyloside-inhibited mitochondrial ADP/ATP carrier of *Saccharomyces cerevisiae*, *J. Biol. Chem. 278*, 36985−36988.
17. Heinze, K. G., Jahnz, M., and Schwille, P. (2004) Triple-color coincidence analysis: One step further in following higher order molecular complex formation, *Biophys. J. 86*, 506−516.
18. Watrob, H. M., Pan, C. P., and Barkley, M. D. (2003) Two-step FRET as a structural tool, *J. Am. Chem. Soc. 125*, 7336−7343.
19. Rostom, A. A., and Robinson, C. V. (1999) Disassembly of intact multiprotein complexes in the gas phase, *Curr. Opin. Struct. Biol. 9*, 135−141.
20. Daniel, J. M., Friess, S. D., Rajagopalan, S., Wendt, S., and Zenobi, R. (2002) Quantitative determination of noncovalent binding interactions using soft ionization mass spectrometry, *Int. J. Mass Spectrom. 216*, 1−27.
21. Nag, N., Krishnamoorthy, G., and Rao, B. J. (2005) A single mismatch in the DNA induces enhanced aggregation of MutS.

Hydrodynamic analyses of the protein−DNA complexes, *FASEB J. 272*, 6228−6243.
22. Medina, R., Perdomo, D., and Bubis, J. (2004) The hydrodynamic properties of dark- and light-activated states of *n*-dodecyl β-D-maltoside-solubilized bovine rhodopsin support the dimeric structure of both conformations, *J. Biol. Chem. 279*, 39565−39573.
23. Fotiadis, D., Liang, Y., Filipek, S., Saperstein, D. A., Engel, A., and Palczewski, K. (2003) Atomic-force microscopy: Rhodopsin dimers in native disc membranes, *Nature (London, U.K.) 421*, 127−128.
24. Palczewski, K. (2006) G protein-coupled receptor rhodopsin, *Ann. Rev. Biochem. 75*, 743−767.
25. Sachs, J. N., and Engelman, D. M. (2006) Introduction to the membrane protein reviews: The interplay of structure, dynamics, and environment in membrane protein function, *Ann. Rev. Biochem. 75*, 707−712.
26. Engelman, D. M. (2005) Membranes are more mosaic than fluid, *Nature (London, U.K.) 438*, 578−580.
27. Arnold, I., Pfeiffer, K., Neupert, W., Stuart, R. A., and Schagger, H. (1998) Yeast mitochondrial F1F0-ATP synthase exists as a dimer: Identification of three dimer-specific subunits, *EMBO J. 17*, 7170−7178.
28. Faye, A., Esnous, C., Price, N. T., Onfray, M. A., Girard, J., and Prip-Buus, C. (2007) Rat liver carnitine palmitoyltransferase 1 forms an oligomeric complex within the outer mitochondrial membrane, *J. Biol. Chem. 282*, 26908−26916.
29. Rabenstein, M. D., and Shin, Y. K. (1995) Determination of the distance between two spin labels attached to a macromolecule, *Proc. Natl. Acad. Sci. U.S.A. 92*, 8239−8243.
30. Borbat, P. P., and Freed, J. H. (2000) Double-quantum ESR and distance measurements, *Biol. Magn. Reson. 19*, 383.
31. Borbat, P. P., Costa-Filho, A. J., Earle, K. A., Moscicki, J. K., and Freed, J. H. (2001) Electron spin resonance in studies of membranes and proteins, *Science (Washington, DC, U.S.) 291*, 266−269.
32. Park, S.-Y., Borbat Peter, P., Gonzalez-Bonet, G., Bhatnagar, J., Pollard Abiola, M., Freed, J. H., Bilwes, A. M., and Crane, B. R. (2006) Reconstruction of the chemotaxis receptor−kinase assembly, *Nat. Struct. Mol. Biol. 13*, 400−407.
33. Milov, A. D., Maryasov, A. G., and Tsvetkov, Y. D. (1998) Pulsed electron double resonance (PELDOR) and its applications in free radical research, *Appl. Magn. Reson. 15*, 107−143.
34. Fafarman, A. T., Borbat, P. P., Freed, J. H., and Kirshenbaum, K. (2007) Characterizing the structure and dynamics of folded oligomers: Pulsed ESR studies of peptoid helices, *Chem. Commun.* 377−379.
35. Jeschke, G. (2002) Distance measurements in the nanometer range by pulse EPR, *Chem. Phys. Phys. Chem. 3*, 927−932.
36. Zhou, Z., DeSensi, S. C., Stein, R. A., Brandon, S., Dixit, M., McArdle, E. J., Warren, E. M., Kroh, H. K., Song, L., Cobb, C. E., Hustedt, E. J., and Beth, A. H. (2005) Solution structure of the cytoplasmic domain of erythrocyte membrane band 3 determined by site-directed spin labeling, *Biochemistry 44*, 15115−15128.
37. Borbat, P. P., McHaourab, H. S., and Freed, J. H. (2002) Protein structure determination using long-distance constraints from double-quantum coherence ESR: Study of T4 lysozyme, *J. Am. Chem. Soc. 124*, 5304−5314.
38. Hilger, D., Jung, H., Padan, E., Wegener, C., Vogel, K. P., Steinhoff, H. J., and Jeschke, G. (2005) Assessing oligomerization of membrane proteins by four-pulse DEER: pH-dependent dimerization of NhaA Na^+/H^+ antiporter of *E. coli*, *Biophys. J. 89*, 1328−1338.
39. Borbat, P. P., Surendhran, K., Bortolus, M., Zou, P., Freed, J. H., and McHaourab, H. S. (2007) Conformational motion of the ABC transporter MsbA induced by ATP hydrolysis, *PLoS Biol. 5*, 2211−2219.
40. Borbat, P. P., and Freed, J. H. (2007) Measuring distances by pulsed dipolar ESR spectroscopy: Spin-labeled histidine kinases, *Methods Enzymol. 423*, 52−116.
41. Milov, A. D., Tsvetkov, Y. D., Formaggio, F., Crisma, M., Toniolo, C., and Raap, J. (2000) Self-assembling properties of membrane-modifying peptides studied by PELDOR and CW-ESR spectroscopies, *J. Am. Chem. Soc. 122*, 3843−3848.
42. Banham, J. E., Timmel, C. R., Abbott, R. J. M., Lea, S. M., and Jeschke, G. (2006) The characterization of weak protein−protein interactions: Evidence from DEER for the trimerization of a von Willebrand factor A domain in solution, *Angew. Chem., Int. Ed. 45*, 1058−1061.
43. Kay, C. W. M., El Mkami, H., Cammack, R., and Evans, R. W. (2007) Pulsed ELDOR determination of the intramolecular distance between the metal binding sites in dicupric human serum transferrin and lactoferrin, *J. Am. Chem. Soc. 129*, 4868−4869.
44. Kay, C. W. M., Elsaesser, C., Bittl, R., Farrell, S. R., and Thorpe, C. (2006) Determination of the distance between the two neutral flavin radicals in augmenter of liver regeneration by pulsed ELDOR, *J. Am. Chem. Soc. 128*, 76−77.
45. Codd, R., Astashkin, A. V., Pacheco, A., Raitsimring, A. M., and Enemark, J. H. (2002) Pulsed ELDOR spectroscopy of the Mo(V)/Fe(III) state of sulfite oxidase prepared by one-electron reduction with Ti(III) citrate, *J. Biol. Inorg. Chem. 7*, 338−350.
46. Bennati, M., Robblee, J. H., Mugnaini, V., Stubbe, J., Freed, J. H., and Borbat, P. P. (2005) EPR distance measurements support a model for long-range radical initiation in *E. coli* ribonucleotide reductase, *J. Am. Chem. Soc. 127*, 15014−15015.
47. Jeschke, G., and Polyhach, Y. (2007) Distance measurements on spin-labeled biomacromolecules by pulsed electron paramagnetic resonance, *Phys. Chem. Chem. Phys. 9*, 1895−1910.
48. Dzikovski, B. G., Borbat, P. P., and Freed, J. H. (2004) Spin-labeled gramicidin A: Channel formation and dissociation, *Biophys. J. 87*, 3504−3517.
49. Berliner, L. J., and McConnell, H. M. (1966) A spin-labeled substrate for α-chymotrypsin, *Proc. Natl. Acad. Sci. U.S.A. 55*, 708−712.
50. Seeley, D., Schleyer, H., Kashiwagi, K., Cooper, D., and Salhanick, H. A. (1987) Studies of the active site of cytochrome P-450scc with a high-affinity spin-labeled inhibitor, *Biochemistry 26*, 1270−1275.
51. Buckman, T., and Eiduson, S. (1980) Studies of pargyline-monoamine oxidase binding using a spin label probe analogue, *J. Neurochem. 34*, 1594−1602.
52. Delannoy, S., Urbatsch, I. L., Tombline, G., Senior, A. E., and Vogel, P. D. (2005) Nucleotide binding to the multidrug resistance P-glycoprotein as studied by ESR spectroscopy, *Biochemistry 44*, 14010−14019.
53. Bode, B. E., Margraf, D., Plackmeyer, J., Durner, G., Prisner, T. F., and Schiemann, O. (2007) Counting the monomers in nanometer-sized oligomers by pulsed electron−electron double resonance, *J. Am. Chem. Soc. 129*, 6736−6745.
54. Newton-Vinson, P., Hubalek, F., and Edmondson, D. E. (2000) High-level expression of human liver monoamine oxidase B in *Pichia pastoris*, *Protein Expr. Purif. 20*, 334−345.
55. Li, M., Hubalek, F., Newton-Vinson, P., and Edmondson, D. E. (2002) High-level expression of human liver monoamine oxidase A in *Pichia pastoris*: Comparison with the enzyme expressed in *Saccharomyces cerevisiae*, *Protein Expr. Purif. 24*, 152−162.
56. Rando, R. R. (1977) The fluorescent labeling of mitochondrial monoamine oxidase, *Mol. Pharmacol. 13*, 726−734.
57. Upadhyay, A. K., Wang, J., and Edmondson, D. E. (2008) Comparison of the structural properties of the active site cavities of human and rat monoamine oxidase A and B in their soluble and membrane bound forms, *Biochemistry 47*, 526−536.
58. Daum, G., Boehni, P. C., and Schatz, G. (1982) Import of proteins into mitochondria. Cytochrome *b*2 and cytochrome *c* peroxidase are located in the intermembrane space of yeast mitochondria, *J. Biol. Chem. 257*, 13028−13033.
59. Daum, G., and Vance, J. E. (1997) Import of lipids into mitochondria, *Prog. Lipid Res. 36*, 103−130.
60. Ramsay, R., Upadhyay, A. K., Li, M., and Edmondson, D. E. (2005) Optical and EPR spectroscopic studies on the anionic flavin radicals in MAOB and its Y435 mutant forms, in *The 15th International Symposium on Flavins and Flavoproteins* (Nishino, T., Miura, R., Tanokura, M., and Kukui, K., Eds.) pp 137−142, ARchiTect Inc., Hayama, Japan.
61. Murib, J. H., and Ritter, D. M. (1952) Decomposition of nitrosyldisulfonate ion. I. Products and mechanism of color fading in acid solution, *J. Am. Chem. Soc. 74*, 3394−3398.
62. Chiang, Y.-W., Borbat, P. P., and Freed, J. H. (2005) The determination of pair distance distributions by pulsed ESR using Tikhonov regularization, *J. Magn. Reson. 172*, 279−295.
63. Chiang, Y.-W., Borbat, P. P., and Freed, J. H. (2005) Maximum entropy: A complement to Tikhonov regularization for determination of pair distance distributions by pulsed ESR, *J. Magn. Reson. 177*, 184−196.
64. Jeschke, G., Panek, G., Godt, A., Bender, A., and Paulsen, H. (2004) Data analysis procedures for pulse ELDOR measurements of broad distance distributions, *Appl. Magn. Reson. 26*, 223−244.

65. Hustedt, E. J., Stein, R. A., Sethaphong, L., Brandon, S., Zhou, Z., and DeSensi, S. C. (2006) Dipolar coupling between nitroxide spin labels: The development and application of a tether-in-a-cone model, *Biophys. J. 90*, 340−356.
66. Milov, A. D., Ponomarev, A. B., and Tsvetkov, Y. D. (1984) Electron−electron double resonance in electron spin echo: Model biradical systems and the sensitized photolysis of decalin, *Chem. Phys. Lett. 110*, 67−72.
67. Jones, T. A., Zou, J. Y., Cowan, S. W., and Kjeldgaard, M. (1991) Improved methods for building protein models in electron density maps and the location of errors in these models, *Acta Crystallogr., Sect. A: Found. Crystallogr. 47*, 110−119.
68. McMahon, H. T., and Gallop, J. L. (2005) Membrane curvature and mechanisms of dynamic cell membrane remodeling, *Nature (London, U.K.) 438*, 590−596.
69. Nury, H., Dahout-Gonzalez, C., Trezeguet, V., Lauquin, G. J. M., Brandolin, G., and Pebay-Peyroula, E. (2006) Relations between structure and function of the mitochondrial ADP/ATP carrier, *Ann. Rev. Biochem. 75*, 713−741.
70. Cramer, W. A., Zhang, H., Yan, J., Kurisu, G., and Smith, J. L. (2006) Transmembrane traffic in the cytochrome *b*6f complex, *Ann. Rev. Biochem. 75*, 769−790.
71. Kim, J., and Raushel, F. M. (2001) Allosteric control of the oligomerization of carbamoyl phosphate synthetase from *Escherichia coli*, *Biochemistry 40*, 11030−11036.
72. Binda, C., Hubalek, F., Li, M., Herzig, Y., Sterling, J., Edmondson, D. E., and Mattevi, A. (2005) Binding of rasagiline-related inhibitors to human monoamine oxidases: A kinetic and crystallographic analysis, *J. Med. Chem. 48*, 8148−8154.
73. Hubalek, F., Binda, C., Khalil, A., Li, M., Mattevi, A., Castagnoli, N., and Edmondson, D. E. (2005) Demonstration of isoleucine 199 as a structural determinant for the selective inhibition of human monoamine oxidase B by specific reversible inhibitors, *J. Biol. Chem. 280*, 15761−15766.

BI7021377